Experimental study and numerical modelling of VHB 4910 polymer

Mokarram Hossain[a], Duc Khoi Vu[a], Paul Steinmann[a,*]

[a] *Chair of Applied Mechanics, University of Erlangen-Nuremberg, Egerlandstr. 5, 91058 Erlangen, Germany*

Abstract

VHB 4910 is an important polymeric material that has potential use as electro-active polymer in producing actuators. Such polymer, a member of the acrylic polymer group, is a very soft viscoelastic material. In this contribution, a comprehensive mechanical characterization of this important viscoelastic material has been carried out using different standard experiments such as single-step relaxation tests, multi-step relaxation tests and loading-unloading cyclic tests. In modelling the mechanical behaviour, a modified version of the micro-mechanically motivated Bergström-Boyce viscoelastic model has been used along with a finite linear evolution law. The model validation shows its excellent capability to predict the experimental results.

Keywords: VHB 4910, viscoelasticity, micro-mechanical model

1. Introduction

In the last couple of decades, one important class of materials that exhibit electro-mechanical couplings is the so-called electronic electro-active polymers (EEAPs), which have potential applications, e.g. as dielectric elastomers (DE) in artificial muscles. EEAPs in actuators are utilized in the form of a thin film that is sandwiched between two electrodes and then exposed to a potential difference, which creates Maxwell forces between the electrodes, i.e. a mechanical output is the resultant due to electric stimuli [1, 27, 28, 39]. VHB 4910 is a potential candidate for use in EEAP actuators. Such material is basically a very soft material that shows

*Corresponding author. Tel.: +49 09131-8528514; Fax: +49 09131-8528503.

Email addresses: mokarram.hossain@ltm.uni-erlangen.de (Mokarram Hossain), vu@ltm.uni-erlangen.de (Duc Khoi Vu), paul.steinmann@ltm.uni-erlangen.de (Paul Steinmann)

physically non-linear viscoelastic behaviour, i.e. it can undergo large deformations with a pronounced dissipative behaviour. A complete mechanical characterization of this important viscoelastic material by various standard experimental tests such as single-step relaxation tests, multi-step relaxation tests, monotonic tests, and loading-unloading cyclic tests at different strain rates and at various extent of deformations is mostly lacking in the literature. In order to pave the way for the modelling of the electro-mechanical coupled behaviour of VHB 4910, first a full-scale mechanical characterization is essential in obtaining a thorough understanding of its behaviour as well as in obtaining a representative mechanical parameter set.

Constitutive models for viscoelastic materials generally fall into two main groups: purely *phenomenological* and *micromechanical* based network models. One can further classify the models based on the nature of the time-dependent part of the stress and also due to the nature of the evolution equation, e.g. integral-based models with stress-type internal variables and differential-type models with strain-type internal variables. Within the phenomenological modelling approaches, one can find models based on stress-type internal variables in the form of convolution integrals in the works of Holzapfel & Simo [31], Simo [35], Lion [36], Kaliske & Rothert [34]. In contrast to the integral-based models, the multiplicative decomposition of the deformation gradient into elastic and inelastic parts yields differential-type viscoelastic models, cf. Huber & Tsakmakis [21], Reese & Govindjee [25]. In both cases, the total stress is decomposed into an equilibrium stress that corresponds to the stress response at an infinitely slow rate of deformation or the stress response when the time-dependent viscous effect is completely diminished and a viscosity-induced overstress. The time-dependent overstress part is then expressed as an integral over the deformation history. Inside the integral expression, a relaxation function is specified as a measure for the materials memory. Due to the thermodynamical consistency requirements, the relaxation function has to follow some restrictions, e.g. it should be positive with negative slope and it has to possess a positive curvature [2, 36]. Within these restrictions, for example, an exponential function or a function based on power laws can be employed. In real polymers, different relaxation times are associated with different segments of the polymer chains. As a result, the long-term relaxation behaviour of polymer using a single exponential function is insufficient. Therefore, in most of the cases, several decreasing exponentials can be superimposed, referred as the so-called Prony series. This approach may produce a large number of material parameters in the model framework that are sometimes difficult to identify.

In contrast to these phenomenological theories, several molecular-based micromechanical theories are available in the literature [8, 13, 15, 22]. These have been developed over the years to describe the viscous behaviour of molten polymers

and physically cross-linked rubber-like materials. The bead-spring model [13], the reptation type tube models [6, 15] and the transient network models [17] can be mentioned as examples in this area. Recently, a growing research activity can be observed to combine these approaches, which yield the so-called micromechanically motivated models [29].

Previous works for modelling the viscoelastic behaviour of VHB 4910 are limited. Several phenomenologically-motivated energy functions, e.g. Neo-Hooke, Mooney-Rivlin, Ogden, Yeoh, are used to model its elastic behaviour. For modelling the time-dependent behaviour, only one work, to the author's knowledge, exists that is in line with the so-called quasi-linear viscoelasticity, i.e. the works of Wissler et al. [37]. In that particular case, the Prony series is used as an approximation of the convolution integral equation, which eventually yields a high number of material parameters. Note that such quasi-linear viscoelasticity is mainly used in bio-mechanics [11]. According to the quasi-linear viscoelasticity assumption, the relaxation function is independent of the imposed deformation in the relaxation test, which might not hold true for all materials. Hence, this assumption can put an extra restriction on the material modelling. Furthermore, the hereditary integral appearing in the formulations is complicated to implement in a research-based in-house code, and it is also difficult to solve analytically. High numbers of material parameters will require extra efforts for identification. Since one of the main future goals of modelling the mechanical behaviour of this polymer is to extend the constitutive model to capture the electro-mechanical coupled behaviour, such quasi-linear viscoelasticity with convolution integral form will probably not be the best alternative. Another approach to model VHB 4910, by using the classical Ogden model, can be found in Gao et al. [38], where the viscoelastic effect is neglected. Moreover, the phenomenological models use empirical relations that usually lack a direct physical interpretation of the governing parameters appearing in the proposed expressions of the energy function [22]. Due to these drawbacks of phenomenologcal models, nowadays the micromechanical models are gaining popularity [5, 8, 9].

The goals of this contribution are manifold, i.e. to present a complete mechanical characterization of VHB 4910 and to apply a thermodynamically consistent physically and geometrically non-linear viscoelastic material model of micro-mechanical type. In a future step, the model will be extended to include the electrostrictive effect with a minimum effort as well as it will be comparatively easier to implement in a research-based finite element (FE) code or in any commercial software package. In this work, the micro-mechanically motivated eight-chain model proposed by Arruda & Boyce [7] for the ground state elastic response of the material and its extension by Linder et al. [29] for the viscoelastic overstress has been adapted. This combination can be termed as the modified version of the Bergström-Boyce

viscoelastic model.
The paper is organized as follows: in Section 2 we briefly outline the experimental set-up, which is utilized to perform the tests in our laboratory. The experimental results are also analysed in this section. Section 3 gives an overview on the constitutive modelling adapted for this material. Therein, the constitutive equations are formulated in one-dimensional form suitable for the parameter identification as well as for the simulation and model validation. In Section 3, the simulations and validation of the model with the experimental data are demonstrated and discussed. Finally, concluding remarks close the paper.

2. Experiments

Two types of VHB acrylic polymers are commercially available, namely VHB 4910 and VHB 4905 where only thickness is a variable, i. e. thickness of 1 mm and 0.5 mm, respectively. In this particular case, we use VHB 4910 due to its larger thickness. These acrylic polymers are produced by $3M$. All tests are carried out at ambient temperature where the undeformed sample geometry is prepared in a way so that the ratio between the length and width should be of 10:1 in order to ensure uniaxial stress condition, cf. Wissler et al. [37]. Two different sample dimensions are used, i.e. 100 mm x 10 mm for the cyclic tests and 50 mm x 5 mm for the relaxation tests. For both cases, the thickness is 1 mm.

2.1. Specimen preparation

Each specimen is captivated at both ends by one pair of aluminium and one pair of plastic plates (two different plates will be required in electrostrictive tests in future) during tests, cf. Fig (1, **a**). Since VHB 4910 is a very soft material, extra precaution is required to prepare a specimen as well as to prepare the clamping plates. Prior to each test, the longer lateral inside edges of the four clamping plates, cf. Fig (1, **a**), are taped by the same VHB 4910 polymer. This type of taping of the plates provides a stronger and uniform clamping of the specimen. Now the red protective film which coats the VHB 4910 polymer needs to be removed. The strips have to be stretched over the lengths of the plates and then, placed and firmly pressed on the back side, cf. Fig (1, **b**). For specimen preparation, with a ruler and a fine liner, two points for a required distance are centrically marked on the surface of the adhesive tape. Again, the red protective coat is removed as straight as possible in order to avoid any twisting or stretching. After that, the sample needs to be positioned on the first clamping plate. During clamping, special care should be given so that the polymeric strip can be placed at the center of the plate hole and perpendicular to the edges of the plates, cf. Fig (1, **c**). After gently pressing the specimen on the first plate, it can now be positioned identically on the second plate. Make sure that

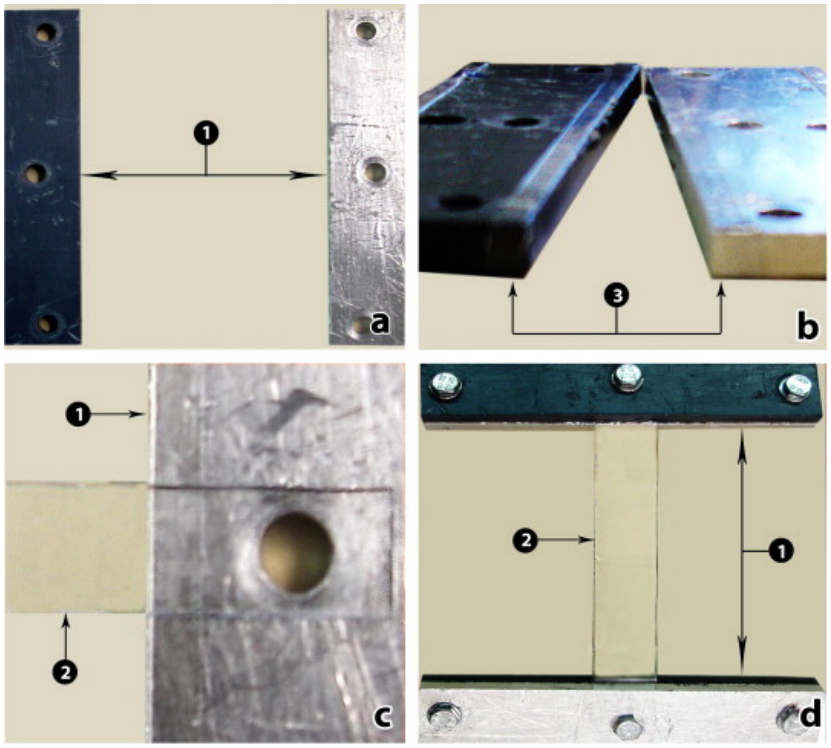

Figure 1: Sample preparation: (**a**) two metal and two plastic plates are used to clamp the specimen, (**b**) taping the plates with the adhesive on their inner sides for better clamping, (**c**) proper placement of the specimen along the holes of the plates for bolting, and (**d**) final clamping of the specimen. Legend: **1**. clamping plates, **2**. specimen, **3**. taped plates

the strip sample is not stretched too much or sags or touches the work surfaces. Once the sample is properly placed on two different plates (one metal and one plastic), the two other plates (one metal and one plastic) are carefully placed to their clamping partners and pressed gently, cf. Fig (1, **d**). To tighten the plates properly, both pairs of the plates are bolted.

2.2. Experimental set-up

As mentioned earlier, a sample is held at its two ends using two pairs of clamps (**1**) of Fig 2, which in turn are mounted on a linear translation stage (**3**) with the help of a table (**4**) and a pair of metal hooks (**5**, **6**). The upper hook (**5**) is connected to the frame (**7**) of the linear translation stage through a force transducer (**8**) (model number GSO-1K, Transducer Techniques). The stretching of the sample (**2**) is realized by moving up and down the table (**3**) using the linear translation stage.

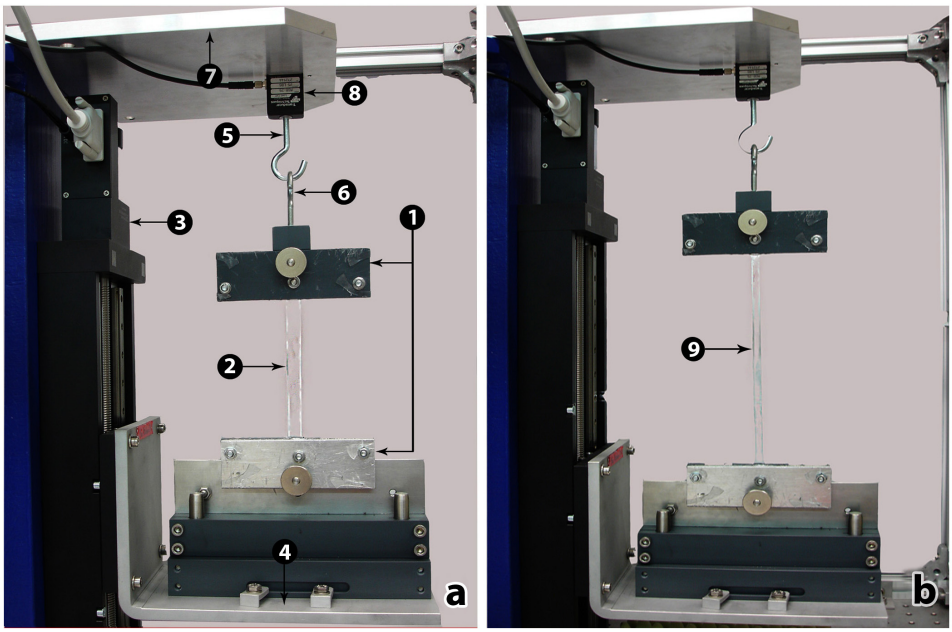

Figure 2: Test preparation: specimen is hanged from the vertically-mounted load cell by a hook in the top; undeformed sample (**a**); Sample is clamped in-between the clamping plates, deformed geometry (**b**). Legend: **1**. clamping plates, **2**. undeformed specimen, **3**. linear stage, **4**. table, **5**. upper hook, **6**. lower hook, **7**. mounting frame, **8**. load cell, **9**. deformed specimen.

During each test, the position of the table is recorded at the same time with the signal captured by the force transducer.

Experiments are conducted either with a constant strain rate as in the cyclic tests or stress relaxation tests at a predefined deformation level. The resulting force history has been measured with the force transducer that can calculate the force signal with a maximum deviation of (precision limit) $\pm$ 0.01 g. The transducer is connected to a PC LabView system for the data acquisition. For each test, at least five specimens are used to assess the degree of reproducibility of the results and one result is chosen as representative. Unless and until stated, all stress calculations are expressed as the nominal stress (first Piola-Kirchhoff stress), i.e. the applied force divided by the original undeformed geometry. The strain rate is defined by $\dot{\varepsilon} = \dot{\Delta L}/L_o$, where L_0 and ΔL denote the initial length and difference between the initial and final lengths of the specimen, respectively. In order to remove noises from the experimental data, a smoothing technique is applied. Note that the limit of our experimental data pool is that these data take into account the typical vis-

coelastic behaviour of the VHB 4910 polymer, i.e. any plasticity or damage such as the Mullins effect is neglected [18].

2.3. Loading-unloading tests

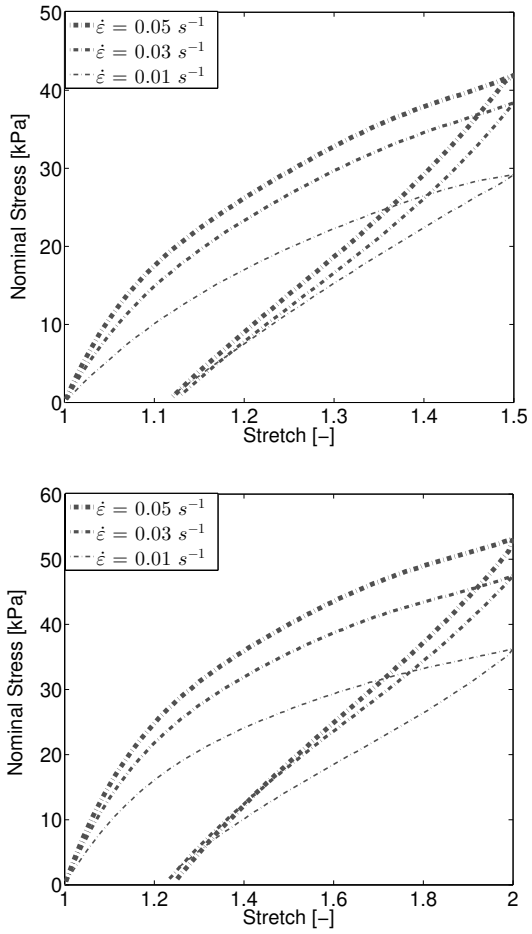

Figure 3: Loading-unloading tests at various strain rates: (**top**) 50% deformation with $0.05s^{-1}$, $0.03s^{-1}$, $0.01s^{-1}$ strain rates; (**bottom**) 100% deformation with $0.05s^{-1}$, $0.03s^{-1}$, $0.01s^{-1}$ strain rates.

The loading-unloading cyclic tests are typical in the case of mechanical characterization of the viscoelastic behaviour of a polymer, i.e. to demonstrate the rate-dependent behaviour of the material. In this particular case, the cyclic tests at

different strain rates and at different stretch levels have been carried out. For this very soft material, strain rates of the range 0.01-0.05s^{-1} reveal best in observing the dissipative behaviour with varied hysteresis loops. Some of these experimental data can be used to identify the viscous material parameters of the selected constitutive model. Tests are carried out at four different extent of deformations, i.e. 50%, 100%, 150% and 200% (stretch levels of 1.5, 2.0, 2.5, and 3.0, respectively), with three different selective strain rates 0.01s^{-1}, 0.03s^{-1}, 0.05s^{-1}. The obtained results are presented in Figs (3) and (4) in terms of nominal stress versus stretch. All experimental results indicate a clearly visible rate-dependent non-linear behaviour during loading but a weaker rate-dependent behaviour during unloading, cf. Fig (3). Such material behaviour could be the effect of the viscosity of the material, cf. Amin et al. [2]. As expected and typical for viscoelastic materials, the area of the resulting hysteresis curves that represents the amount of dissipated energy per cycle gets larger as the loading rate increases from 0.01s^{-1} to 0.05s^{-1}. These data show that the material viscosity parameter is nonlinear and is sensitive to strain-rate, see also Vandenbroucke et al. [4]. Moreover, the presence of a hysteresis loop along with a permanent set (the amount of deformation which is not recovered even after full unloading) is clearly visible in each test, cf. Fig (3).

2.4. Multi-step relaxation

To determine the basic elasticity of the material, i.e. the equilibrium response, several alternatives are proposed in the literature, the multi-step relaxation test is one of them. Certain authors [2, 18] suggested to compute the equilibrium response by performing tests at an infinitely slow rate, but in practical cases, due to presence of unknown amount of viscosity in the materials it is difficult to identify a specific loading rate which is slow enough to obtain the equilibrium responses. To ameliorate this difficulty and also to produce adequate data pool to verify the proposed constitutive model, multi-step relaxation tests at various level of deformations have been performed. A deformation velocity of 100 mms^{-1}, which is the maximum machine speed in our case, followed by a holding time of thirty minutes in each step of the deformation has been utilized. The step-wise load history is demonstrated in Fig (5, **top**). It can be observed that at the end of each step stretching with a holding period of thirty minutes, the stress converges to an almost constant state. Thirty minutes holding period for the relaxation experiments of the VHB 4910 polymer is also used in the works of Wissler el al. [37]. Note that a rapid stress relaxation is observed within the first few seconds and after that the stress approaches asymptotically towards an equilibrium state. Although the equilibrium response is obtained in an asymptotic sense, such stress states are widely recognized as the equilibrium stresses at respective stretch levels in the literature [2, 36]. More discussions can be found in Section 3.2. The experimental data that depict

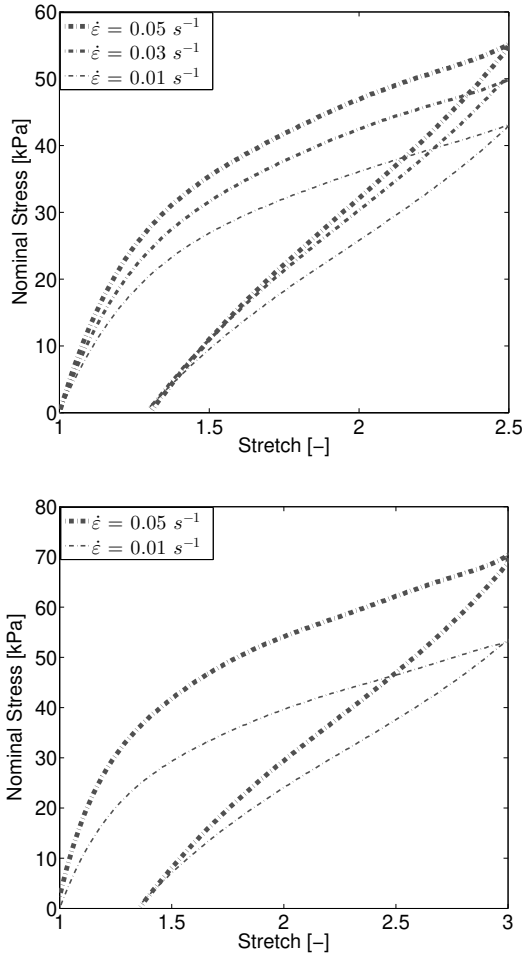

Figure 4: Loading-unloading experiments at various strain rates: (**top**) 150% deformation with $0.05s^{-1}$, $0.03s^{-1}$, $0.01s^{-1}$ strain rates; (**bottom**) 200% deformation with $0.05s^{-1}$, $0.01s^{-1}$ strain rates.

nominal stress response over time are presented in Fig (5, **bottom**). The remaining experiments have been carried out to produce more data in order to validate the model.

2.5. Single-step relaxation

Another frequently used option to determine the equilibrium stress response, i.e. time-independent stress, as well as to observe time-dependent viscous behaviour

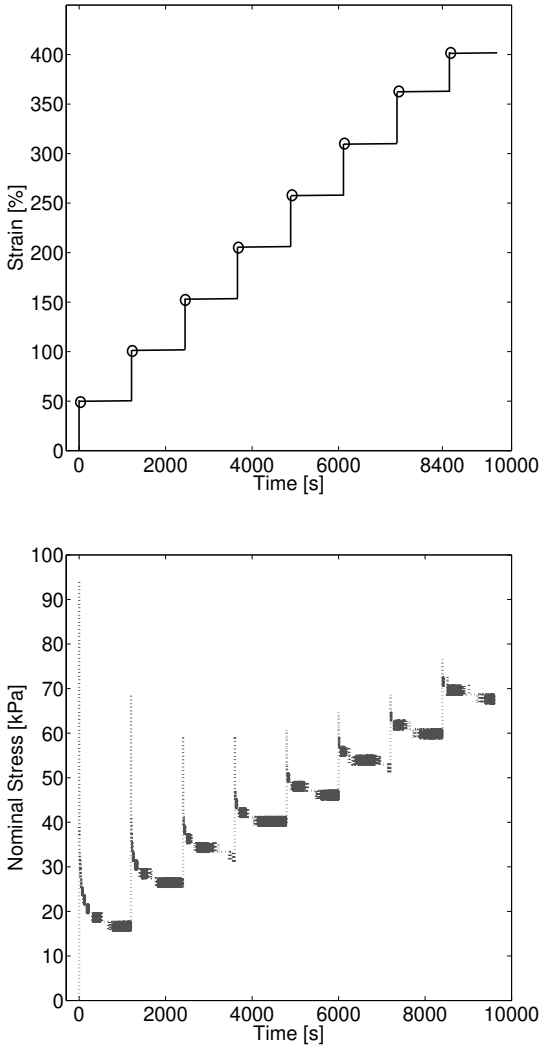

Figure 5: Multi-step relaxation tests: Step-wise stretches during tests (**top**), stress relaxations at 50% deformation in each step (**bottom**, unsmoothed data)

of the material is the single-step relaxation tests at various stretch levels. In this case, the single-step relaxation experiments at various deformations have been performed. During the application of load, a deformation velocity of 100 mms^{-1} has been used. The holding time for stress relaxation is thirty minutes in all tests de-

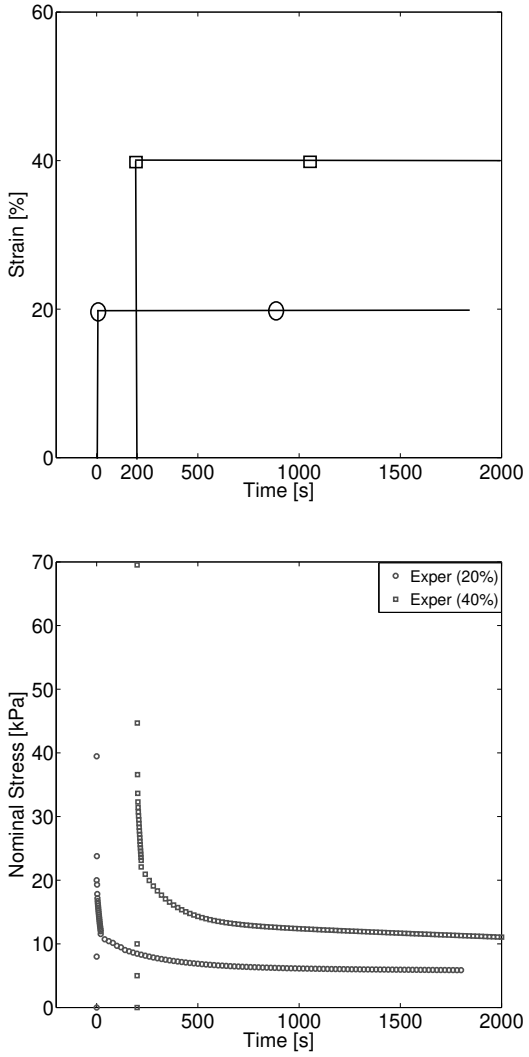

Figure 6: Single-step relaxation tests at 20% (**circle**) and 40% (**rectangle**) strains. For better illustration, the stress and strain histories for two strains have been separated from each other by 200s.

scribed in the section. Because of space constraint, only few experimental data out of many single-step relaxation test data are presented in Figs (6) and (7). It can be observed that at the end of a single-step relaxation test with a holding period of thirty minutes, the stress converges to an almost constant state. Simliar to

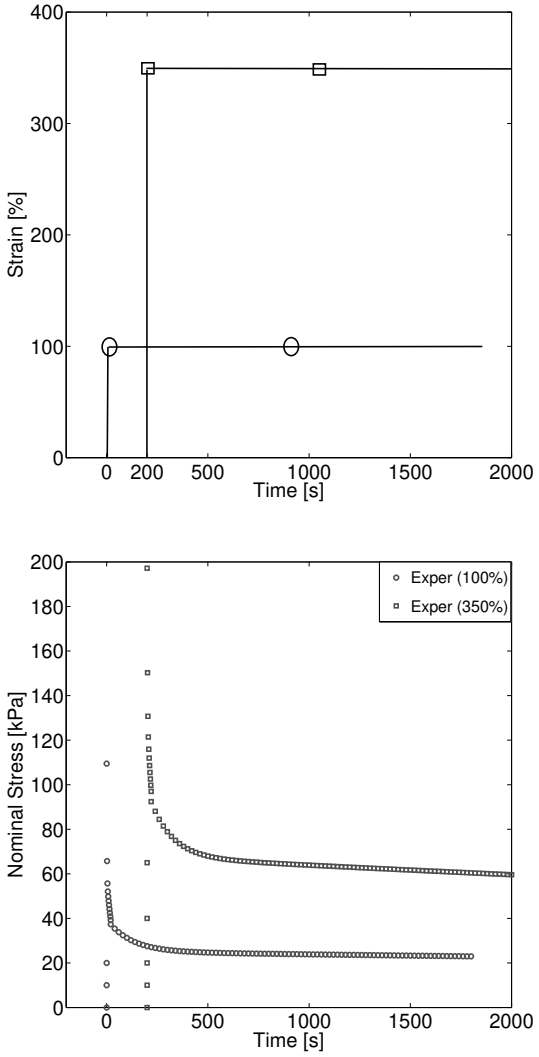

Figure 7: Single-step relaxation tests at 100% (**circle**) and 350% (**rectangle**) strains. For better illustration, the stress and strain histories for two strains have been separated from each other by 200s.

the multi-step relaxation tests, a rapid stress relaxation can be observed within the first few seconds and the stress measured at the end point of a relaxation time can be considered as the value of the equilibrium stress. The difference between the current stress and the equilibrium stress is the so-called overstress, cf. Amin et

al. [2]. More discussions will follow in Section 3.2. When the results obtained at various strain levels are compared, it can be observed that higher strain levels produce larger overstresses than those at lower strain levels with lower overstresses. These revelations need to be considered during the development of the constitutive model.

3. Constitutive modelling and simulation

In this section, a micro-mechanically motivated finite strain viscoelastic model is presented, which is a modified version of the Bergström-Boyce model. Since the experimental results produced in the previous section are from uniaxial tests, after a brief overview on the model, the one-dimensional version of the model is formulated. In micromechanical modelling approaches for polymers, statistical mechanics is used to obtain micro-level information, which is then transferred to the macro level by averaging or homogenization. This homogenization can be achieved either by an affinity or non-affinity assumption. The three-chain, four-chain, eight-chain, and micro-sphere models are different ways to think of the averaging procedure from micro to macro levels. Needless to mention that the non-Gaussian theory, in contrast to the Gaussian one, leads to a more realistic molecular distribution function valid over the whole range of r-values (end-to-end distance) up to the ultimate or fully extended length. Several micro-mechanically motivated network models for hyperelastic materials have been proposed in the literature [7], for review and more details, see Marckmann & Verron [26], Miehe et al. [22, 23], Hossain [32], Steinmann et al. [33].

3.1. Modelling

The kernel in the finite strain constitutive modelling is the energy function. In the case of viscoelasticity, it is assumed that the total energy function depends on the deformation and internal variables, i.e.

$$\Psi = \tilde{\Psi}(\boldsymbol{C}, \boldsymbol{A}_1, \cdots, \boldsymbol{A}_s) \tag{1}$$

where s denotes the number of elements which form the relaxation spectrum. In Eqn (23), $\boldsymbol{C}$ and $\boldsymbol{A}_i$ denote the right Cauchy-Green strain tensor and tensorial internal variables, respectively. Since polymeric materials are treated as nearly incompressible materials, for numerical purpose, the total free energy can be decomposed into volumetric and isochoric contributions. Further, the isochoric contribution will be decomposed into elastic and viscous parts as

$$\Psi(\boldsymbol{C}, \boldsymbol{A}) = \tilde{\Psi}_{vol}(J) + \tilde{\Psi}_{iso}(\bar{\boldsymbol{C}}, \boldsymbol{A}) = \tilde{\Psi}_{vol}(J) + \tilde{\Psi}^{e}_{iso}(\bar{\boldsymbol{C}}) + \sum_{i=1}^{s} \tilde{\Psi}^{v}_{iso,i}(\bar{\boldsymbol{C}}, \boldsymbol{A}_i) \tag{2}$$

where $J = \det\boldsymbol{F}$, $\bar{\boldsymbol{C}} = J^{-2/3}\boldsymbol{C}$. Each member of the relaxation spectrum roughly represents a Maxwell element. Similar to the decoupled representation of the energy function, the corresponding decoupling of the stress tensor yields

$$\boldsymbol{S} = \boldsymbol{S}_{vol} + \boldsymbol{S}_{iso} = 2\frac{\partial \Psi_{vol}}{\partial \boldsymbol{C}} + 2\frac{\partial \Psi_{iso}}{\partial \boldsymbol{C}}. \tag{3}$$

In Eqn. (3), we have $\boldsymbol{S}_{vol} = Jp\boldsymbol{C}^{-1}$, where the hydrostatic pressure $p = \partial \Psi_{vol}(J)/\partial J$ has been introduced. For compressible materials, several proposals for the volumetric part of the energy function (Ψ_{vol}) have been made, cf. Holzapfel [31]. In the case of incompressibility, $J = 1$ and p serves as a Lagrange multiplier to satisfy this kinematic constraint on the deformation field. The isochoric energy function Ψ_{iso} is expressed in terms of the isochoric right Cauchy-Green tensor $\bar{\boldsymbol{C}} = \bar{\boldsymbol{F}}^t\bar{\boldsymbol{F}}$, $\bar{\boldsymbol{F}} = J^{-1/3}\boldsymbol{F}$. The definition of the stress tensor $\bar{\boldsymbol{S}} = 2\partial \Psi_{iso}(\bar{\boldsymbol{C}}, \boldsymbol{A})/\partial \bar{\boldsymbol{C}}$ is introduced and the isochoric stress $\boldsymbol{S}_{iso}$ is related to the previous one via the fourth-order projection tensor $\mathbb{P} = \partial \bar{\boldsymbol{C}}/\partial \boldsymbol{C}$ by

$$\boldsymbol{S}_{iso} = J^{-\frac{2}{3}}\mathbb{P} : \bar{\boldsymbol{S}} \qquad \text{with} \qquad \mathbb{P} = \mathbb{I} - \frac{1}{3}\boldsymbol{C}^{-1} \otimes \boldsymbol{C} \quad , \quad \mathbb{I}_{ijkl} = \delta_{ik}\delta_{jl} \tag{4}$$

where δ_{ij} is a Kronecker delta. The stress $\bar{\boldsymbol{S}}$ is further decomposed into elastic and viscous parts, i.e. $\bar{\boldsymbol{S}} = \bar{\boldsymbol{S}}^e + \bar{\boldsymbol{S}}^v$. Each stress mentioned above requires a separate energy function to have a complete representation. A micro-mechanically motivated energy function for the ground state elasticity and a potential function for the viscous overstress are elaborated and their corresponding stress tensors are derived in the following.

The eight-chain model [7] is a classical and successful constitutive framework for the modelling of polymeric materials. This constitutive model is based on an eight chain representation of the underlying macromolecular network structure of polymers, which uses the non-Gaussian behaviour of the individual chains. It is revealed that this model accurately captures the ultimate strain of network deformation while requiring only two material parameters, the shear modulus (μ) and the number of segments per chain (N). Incorporation of the Langevin model for the statistics of an individual chain, the isochoric part of the free energy can be obtained [7, 33] as

$$\Psi^e_{iso}(\bar{\boldsymbol{C}}) = \mu N \left[\bar{\gamma}\bar{\lambda}_r + \ln\left[\frac{\bar{\gamma}}{\sinh\bar{\gamma}}\right]\right], \tag{5}$$

with the relative chain stretch $\bar{\lambda}_r = \frac{\bar{\lambda}}{\sqrt{N}} = \sqrt{\frac{\bar{I}_1}{3N}}$, where $\bar{I}_1$ is the first invariant of the isochoric part of the right Cauchy-Green tensor $\bar{\boldsymbol{C}}$. In Eqn (5) $\bar{\gamma}$ is the inverse Langevin function that can be approximated via the Padé approximation,

i.e. $\bar{\gamma} \approx \bar{\lambda}_r \frac{3-\bar{\lambda}_r^2}{1-\bar{\lambda}_r^2}$, due to better accuracy. From equation (3) and using the relation in (5), the elastic part of the stress tensor can be calculated:

$$\bar{\boldsymbol{S}}^e = \frac{\mu}{3}\left[\frac{3N-\bar{\lambda}^2}{N-\bar{\lambda}^2}\right]\boldsymbol{I}, \qquad \boldsymbol{I}_{ij} = \delta_{ij}. \tag{6}$$

Now the remaining part of the constitutive model is to find a suitable micro-mechanically motivated energy function for the viscous part and an evolution equation for the internal variable. Very recently, Linder and co-workers [29] re-interpreted the micro-mechanical origin of the viscoelastic energy function and the evolution law proposed by Lubliner [30]. They departed from the so-called Smoluchowski equation for the diffusion problem and surprisingly came up with the same formulation for the viscous energy function and evolution equation that were proposed earlier by Lubliner exploiting the works of Green and Tobolsky [17], i.e.

$$\Psi^v_{iso} = \sum_{i=1}^{s} \tilde{\Psi}^v_{iso,i}(\bar{\boldsymbol{C}}, \boldsymbol{A}_i) = \sum_{i=1}^{s} \frac{1}{2}\mu_i^v \left[(\boldsymbol{A}_i : \bar{\boldsymbol{C}} - 3) - \ln\det(\boldsymbol{A}_i)\right] \tag{7}$$

where μ_i^v is a viscous shear modulus and $\boldsymbol{A}_i$ are the strain-like tensorial variables associated with viscous Maxwell elements. A thermodynamically consistent evolution ansatz for the internal variable of a single element follows

$$\dot{\boldsymbol{A}}_i = \frac{1}{\tau_i}\left[\bar{\boldsymbol{C}}^{-1} - \boldsymbol{A}_i\right], \tag{8}$$

where τ_i is the relaxation time. For proof of the thermodynamical consistency, see Appendix A. Note that such finite strain evolution law is of linear type, which is contrast to the non-linear finite strain evolution laws proposed by Sedlan [12], Reese & Govindjee [25], Amin et al. [2], Koprowski et al. [19, 20]. Due to its simplicity, this particular evolution law has been chosen initially and the application of a non-linear evolution ansatz could be a subject of future research for this material. Using the definition in Eqn (4), the viscous overstress can be found as

$$\bar{\boldsymbol{S}}^v_i = 2\frac{\partial \Psi^v_{iso,i}}{\partial \bar{\boldsymbol{C}}} = \mu_i^v \boldsymbol{A}_i. \tag{9}$$

All of the tests presented in Section 2 are of uniaxial type. Therefore, the constitutive model discussed above needs to be formulated in one-dimensional form in order to identify the material parameters as well as to validate the applied model. As per definition of a uniaxial tension test, the specimen is elongated only in one direction, i. e. $\lambda_1 = \lambda$ while the other two directions are free to move. From the incompressibility condition, i. e. $\det\boldsymbol{F} = \det\bar{\boldsymbol{F}} = \lambda_1\lambda_2\lambda_3 = 1$ and the assumption

of symmetry the complementary principal stretches follow as $\lambda_2 = \lambda_3 = \lambda^{-1/2}$. Therefore, the complete deformation gradient ($\boldsymbol{F}$) reads

$$\boldsymbol{F} = \begin{bmatrix} \lambda & 0 & 0 \\ 0 & \lambda^{-1/2} & 0 \\ 0 & 0 & \lambda^{-1/2} \end{bmatrix}. \tag{10}$$

Note that since the elongation is only in one direction, the specimen will contract in the transversal directions and due to the stress-free boundary conditions, both nominal stresses P_2 and P_3 are zero and only nominal stress P_1 needs to be determined. Inserting all this information in Eqn (6), the elastic part of the nominal stress is obtained:

$$P^e = \frac{\mu}{3}\left[\frac{3N - \lambda_{cu}^2}{N - \lambda_{cu}^2}\right]\left[\lambda - \lambda^{-2}\right], \qquad \lambda_{cu} = \sqrt{\frac{1}{3}\left[\lambda^2 + \frac{2}{\lambda}\right]}, \tag{11}$$

for details, see Hossain [32], Steinmann et al. [33]. Now, the viscous part of the stress for a single Maxwell element is formulated (assuming incompressibility condition for the internal variable $\boldsymbol{A}_i$) from Eqns (8) and (9):

$$P^v = \sum_{i=1}^{s} P_i^v = \sum_{i=1}^{s} \mu_i^v \left[\lambda \lambda_i^{2,A} - \frac{1}{\lambda^2 \lambda_i^A}\right], \tag{12}$$

where $\lambda_i^{2,A}$ is the principal stretch of the internal variable $\boldsymbol{A}_i$. Combining Eqns (11) and (12), the total stress can be obtained as

$$P = \frac{\mu}{3}\left[\frac{3N - \lambda_{cu}^2}{N - \lambda_{cu}^2}\right]\left[\lambda - \lambda^{-2}\right] + \sum_{i=1}^{s} \mu_i^v \left[\lambda \lambda_i^{2,A} - \frac{1}{\lambda^2 \lambda_i^A}\right], \tag{13}$$

where $\lambda_{cu} = \sqrt{\frac{1}{3}\left[\lambda^2 + \frac{2}{\lambda}\right]}$. Similar to the one-dimensional formulation of the total stress, the evolution law is derived:

$$\dot{\lambda_i^{2,A}} = \frac{1}{\tau_i}\left[\lambda^{-2} - \lambda_i^{2,A}\right]. \tag{14}$$

This scalar-valued differential equation needs to be discretized by a suitable integration scheme. Discretizing by the unconditionally stable implicit Euler-backward integration scheme, the differential equation for the internal variable λ^A for a single Maxwell element yields

$$\begin{aligned} \lambda^A &= \lambda^{n,A} + \frac{\Delta t}{2\tau}\left[\frac{\lambda^{-2} - \lambda^{2,A}}{\lambda^A}\right] \\ f(\lambda^A) &= \lambda^A - \lambda^{n,A} - \frac{\Delta t}{2\tau}\left[\frac{\lambda^{-2} - \lambda^{2,A}}{\lambda^A}\right] \end{aligned} \tag{15}$$

where $[\bullet]^i = [\bullet]\,(t_i)$ and $\Delta t = t_{n+1} - t_n$. For the sake of brevity, the index for the current value (t_{n+1}) of the stretch λ^A has been dropped in Eqn (15). Eqn (15) is non-linear in terms of λ^A. Therefore, a Newton-type iterative scheme is required to find the current value of λ^A that need to be inserted in Eqn (13) to obtain the updated value of the total stress $P(t)$.

3.2. Parameter identification and simulation

The first step for parameter identification is to identify the material parameters for the basic (ground state) elasticity, i.e. the so-called equilibrium stress response. Several alternatives are proposed in the literature [2, 16, 18, 36] to separate the basic elasticity from the time-dependent stress responses in experimental data:

- The first option for obtaining the basic elasticity could be the single-step relaxation tests. The values of the stresses that reach asymptotically at the end of each holding time for each deformation level are considered as the equilibrium stresses, cf. Figs (6) and (7).

- Another possibility is to take the asymptotic stresses from the multi-step relaxation tests. The application of a step elongation followed by a certain holding period will help to decrease the stress response gradually to an asymptotical end, cf. Fig (5).

- The third alternative is based on the loading-unloading cyclic tests. By carrying out a repeated number of cyclic tests at a particular strain, a stationary hysteresis loop can be obtained. Then, the average of the last loading and unloading curves are identified as the basic elasticity for that particular strain level.

- The fourth option is to perform monotonic tests at a sufficiently slow rate. This can produce equilibrium stress (quasi-elastic stress) responses. Such tests could provide enough time to the material to be relaxed during loading. Experimental results at the slowest rates will diminish the viscous effect from the materials and only the equilibrium response will survive.

To identify the basic elasticity in this particular case, the first two options have been selected. Equilibrium data are presented in Fig (8, **top**), i.e. asymptotic stress values from the single-step relaxation tests and asymtotic stresses from the multi-step relaxation tests. The other two options to obtain the basic elasticity cannot be explored due to high viscoelastic behaviour of the material and our machine limitation. Since the experimental results from the two different options produce almost similar results, we choose to follow the representative value of the multi-step relaxation tests after thirty minutes holding time in each step-wise test. The

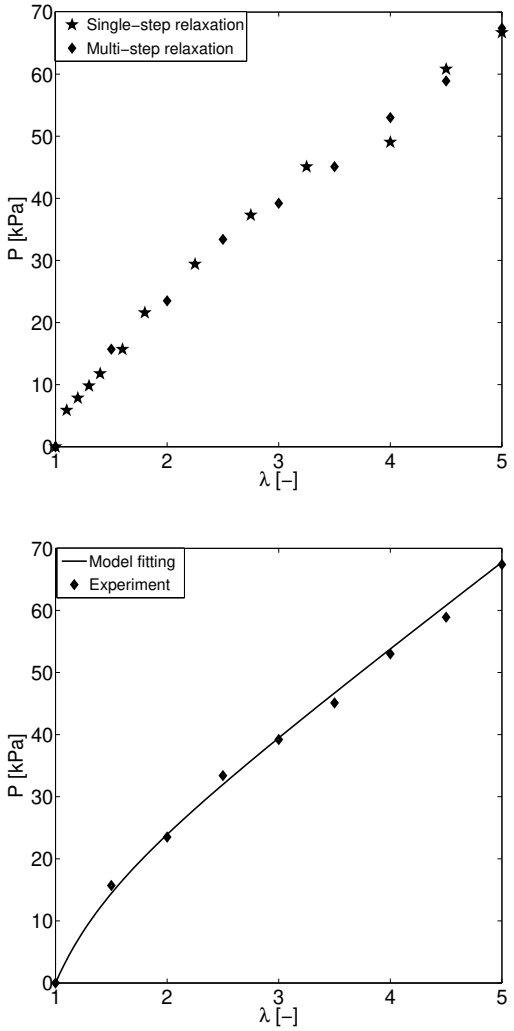

Figure 8: Identification of the elastic material parameters from the basic elasticity data: Equilibrium stresses from the single-step and multi-step relaxations tests (**top**), model fitting with the multi-step relaxation test data only (**bottom**)

one-dimensional elastic stress-stretch equation (11) is then fitted to the experimental data in Fig (8, **bottom**) and the optimized elastic parameters μ, N are obtained to be $[\mu, N]$=[13.65 kPa, 7.84e05].

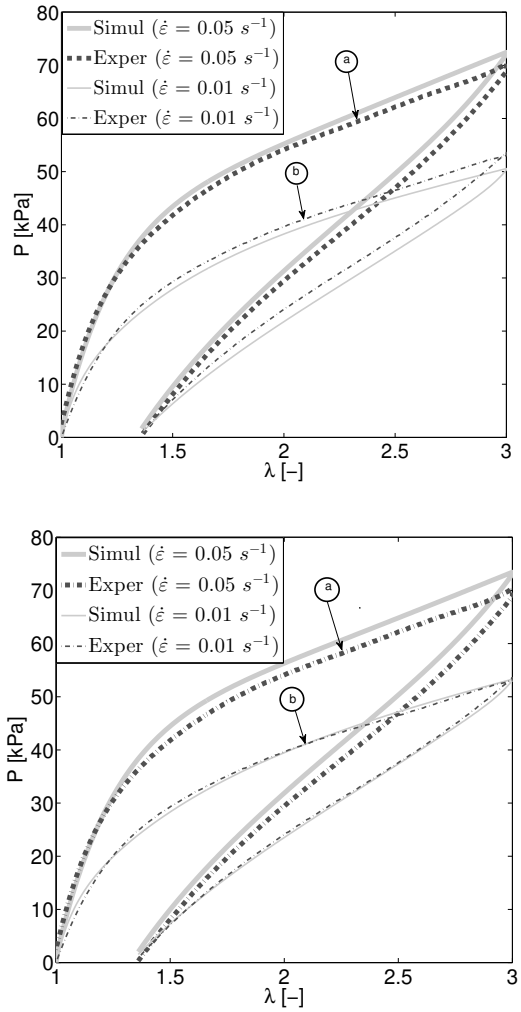

Figure 9: Fitting for 200% deformation at two different strain rates simultaneously. Fitting using four Maxwell elements (**top**) and five Maxwell elements (**bottom**), respectively

Now, the remaining problem of the parameter identification is to identify the viscous parameters. For the representation of the real relaxation spectrum several viscous branches, which are equivalent to several Maxwell elements, need to be considered. In particular, to fit the experimental data presented in previous section, a discrete spectrum of relaxation times and overstress moduli, i.e. $\{\tau_i\}_{i=1}^{s}$ and $\{\mu_i^v\}_{i=1}^{s}$ are chosen, respectively. With a spectrum of relaxation times, i.e. with

several Maxwell elements (each Maxwell element produces two extra parameters), an optimized set of material parameters is identified from a strain rate of $0.05s^{-1}$ at 200% deformation. The first step in the viscoelastic parameter identification of the VHB 4910 polymer is to determine the number of Maxwell elements required to capture the non-linear viscoelastic behaviour of this material. It is observed that a set of four Maxwell elements is enough to capture the behaviour with a fair accuracy, cf. Fig (9). Note that the identified parameter set for $0.05s^{-1}$ strain rate is neither predicting the data at another strain, e.g. $0.01s^{-1}$ of the same deformation (200%) nor at another deformation (say, 100%). Therefore, experimental data for the two different strain rates at 200% deformation, $0.05s^{-1}$ and $0.01s^{-1}$ in our case, are set in the objective function. This procedure, in the literature, is sometimes called the *simultaneous minimization* for the parameter identification [3, 29]. The frequently used method for the simultaneous minimization is summarized in the following. Once the ground state elastic part of the stresses is obtained through the eight-chain model, the remaining parameters that need to be determined are the overstress moduli $\{\mu_i^v\}_{i=1}^s$ and the relaxation spectrum $\{\tau_i\}_{i=1}^s$. For this particular case, the total stress is computed based on

$$P(t) = P^e + \sum_{i=1}^{s} P_i^v(t) \tag{16}$$

where P^e and $\{P_i^v\}_{i=1}^s$ are the elastic equilibrium stress and the viscous overstresses, respectively. As stated earlier, we take two different strain rates in the minimization process that can be denoted by the indices a, b in the cyclic tests in Fig (9). Now, the total stress can be expressed as a simple combination

$$P^{ab}(t) = P^{e,ab} + \sum_{i=1}^{s} \mu_i^v \tilde{P}_i^{v,ab}(t). \tag{17}$$

In Eqn (17), $\tilde{P}_i^{v,ab}(t)$ are the normalised overstresses that can be computed separately for each of the s branches with a unit moduli assigned as $\{\tilde{\mu}_i^v\} = 1$ kPa and the loading rates corresponding to the cyclic tests a, b, presented in Fig (9). The overstress moduli $\{\mu_i^v\}_{i=1}^s$ and the relaxation spectrum $\{\mu_i^v\}_{i=1}^s$ are then obtained by minimizing the discrepancy between the stress-strain curves from the experiments and the simulations. Note that during identification of the viscoelastic parameters, the elastic parameters μ, N determined earlier are kept frozen. The optimized parameter set using the `Matlab` built-in optimization routine `lsqnonlin` is summarized in Table 1. The fittings with four and five Maxwell elements are

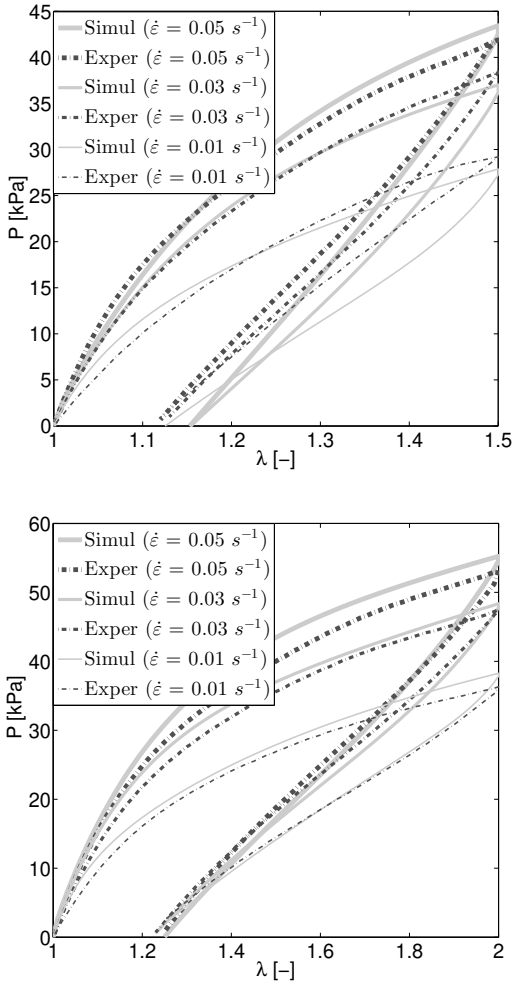

Figure 10: Validation for 50% (**top**) and 100% (**bottom**) deformations at three different strain rates, $0.05s^{-1}$,$0.03s^{-1}$ and $0.01s^{-1}$.

shown in Fig (9, **top**) and Fig (9, **bottom**), respectively, which depict that the increase of Maxwell elements from four to five does not significantly improve the fitting quality. Therefore, the identified parameters for the four Maxwell elements are taken as the optimized parameters, cf. Table 1.

Now, the complete set of optimized viscoelastic parameters obtained from 200% deformation data is used to validate the model with other experimental data, which

Table 1: Identified elastic and viscoelastic material parameters, respectively; μ, μ_i^v in [kPa] and τ_i in [s]

μ	N	μ_1^v	μ_2^v	μ_3^v	μ_4^v
13.65	7.84e+05	120.78	37.02	7.061	13.155
-	-	τ_1	τ_2	τ_3	τ_4
-	-	0.055	5.172	1.6e-06	96.769

are not included during the identification procedure. The validation results for 50%, 100%, and 150% deformations at strain rates of $0.05s^{-1}$, $0.03s^{-1}$ and $0.01s^{-1}$ are presented in Fig (10) and Fig (12, **top**). All validation examples show excellent agreements with the data. Only a small discrepancy in the case of $0.01s^{-1}$ strain rate of 150% deformation is observed.

Data from the single-step relaxation and multi-step relaxation experiments need to be validated with the same set of parameters identified earlier. The validation with four single-step relaxation data sets, i.e. 20%, 40%, 100% and 350% is presented in Figs (11, **top**) and (11, **bottom**). More validation examples for this type of tests are discarded here due to space constraint. The numerical validation illustrates good agreements between experimental data and simulation except a small discrepancy in capturing the bended part. In the case of single-step relaxation test data, the model captures perfectly even the stress-peak values at the beginning of the experiments, see Fig (11). Furthermore, the multi-step relaxation data are simulated, which also show satisfactory agreements, see Fig (12, **bottom**). Note that both in single- and in multi-step relaxations, prediction of the bended part is not exact. According to several authors, such minor inaccuracy can be improved by applying non-linear viscosity functions in the evolution ansatz, cf. Sedlan [12], Amin et al. [2], Zrida et al. [10], Koprowski et al. [19]. It is interesting to note that at higher strain, the development of the overstresses from the model matches the experimental data very well.

4. Summary and outlook

In this contribution, an illustrative sketch on the mechanical characterization of VHB 4910 polymer by various standard tests is presented. For the modelling of this extremely soft polymer, a thermodynamically consistent modified version of the Bergström-Boyce viscoelastic model is adapted with a finite strain linear evolution law. The fitting and validation examples represent quite good agreements. A small discrepancy in capturing the curvature parts of the stresses in the relaxation examples could possibly be improved by using a finite non-linear evolution ansatz.

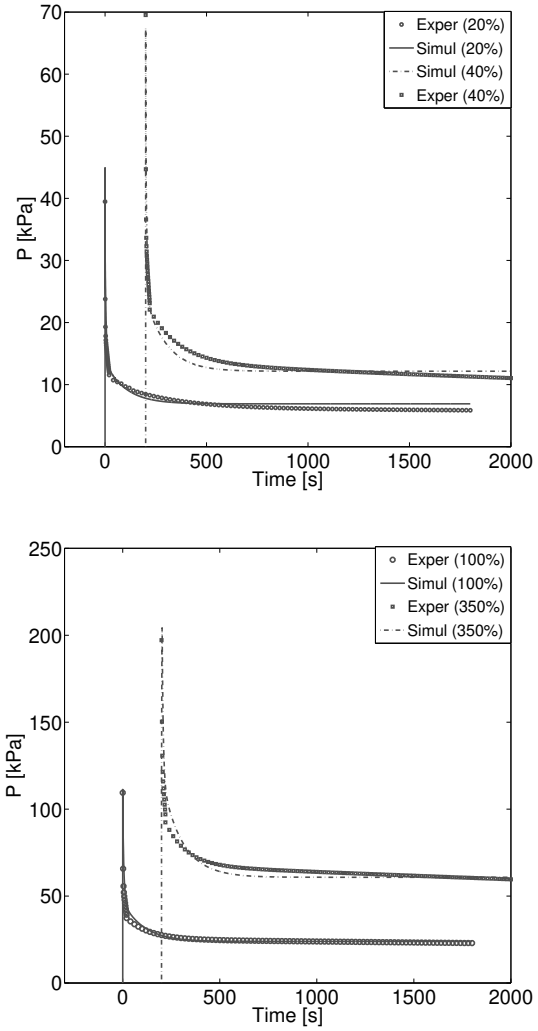

Figure 11: Validation for the single-step relaxation data. (**Top**) Single-step relaxation of 20% and 40% strains with thirty minutes holding time; (**bottom**) Single-step relaxation of 100% and 350% strains for thirty minutes holding time. For better illustration and understanding, the stress and strain histories for two strains have been separated from each other by 200 s

Further works in this direction will be the use of a more advanced energy function other than a Neo-Hookean function in the viscous part as well as modelling the experimental data after performing the Mullins effect on the virgin specimens.

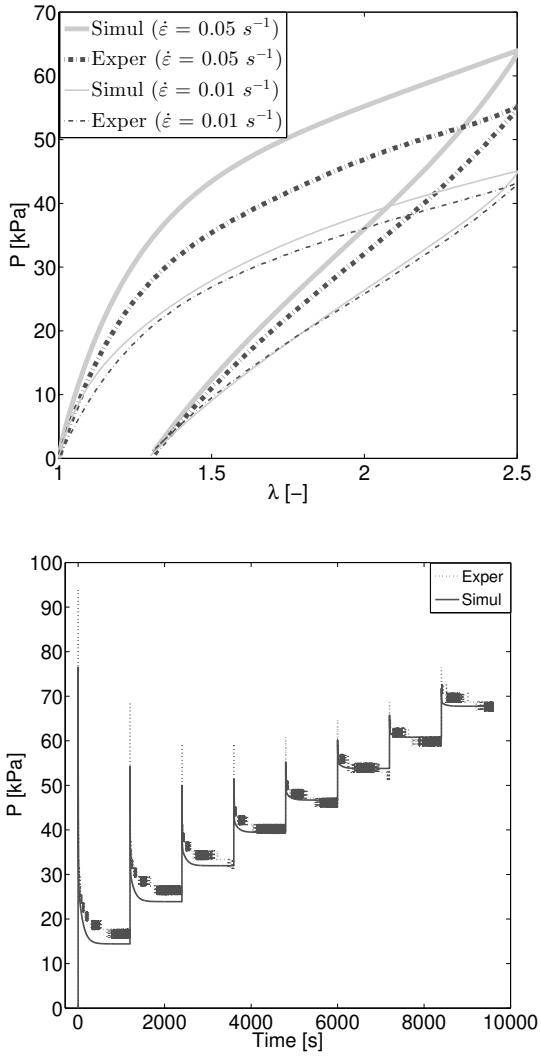

Figure 12: Comparison between model and experimental data for the 150% deformation at two different strain rates (**top**). Validation for the multi-step relaxation tests; 50% deformation in each step (**bottom**, unsmoothed data). Holding time for step-wise relaxation test is twenty minutes

Such advanced evolution law and energy function could capture the experimental data in a more realistic way. In a forthcoming contribution, this modelling approach will be extended to incorporate the electric effect in the case of coupled

electro-mechanical problem.

Acknowledgements The authors greatfully acknowledge the financial support of the German Research Foundation (DFG) within the project "Electronic electroactive polymer under electric loading: Experiment, modelling and simulation", Grant No. STE 544/36-1.

Appendix A: Thermodynamical consistency of the viscoelastic model

The constitutive relations presented in Eqns (7-9) are required to fulfill the entropy inequality, which, if only isothermal processes are considered, is equal to the so-called dissipation inequality, i.e.

$$\boldsymbol{S} : \frac{1}{2}\dot{\boldsymbol{C}} - \dot{\Psi} \geq 0. \tag{18}$$

If one performs the time derivative of the total energy, i.e. $\tilde{\Psi}(\boldsymbol{C}, \boldsymbol{A}_1, \cdots, \boldsymbol{A}_s)$ and inserts it in Eqn (18), we obtain

$$\left[\boldsymbol{S} - 2\frac{\partial \Psi}{\partial \boldsymbol{C}}\right] : \frac{1}{2}\dot{\boldsymbol{C}} - \sum_{i=1}^{s} \frac{\partial \Psi}{\partial \boldsymbol{A}_i} : \dot{\boldsymbol{A}}_i \geq 0. \tag{19}$$

To obtain a thermodynamically consistent formulation that obeys the second axiom of thermodynamics the local dissipation has to be non-negative, which, due to Coleman and Gurtin argumentation [14] yields

$$\mathcal{D}_{loc} = -\sum_{i=1}^{s} \frac{\partial \Psi}{\partial \boldsymbol{A}_i} : \dot{\boldsymbol{A}}_i = -\sum_{i=1}^{s} \frac{\partial \bar{\Psi}^{v}_{iso,i}}{\partial \boldsymbol{A}_i} : \dot{\boldsymbol{A}}_i = \sum_{i=1}^{s} \mathcal{D}_{loc,i} \geq 0. \tag{20}$$

Performing the derivation of the viscous part of the energy function from Eqn (7) along with the evolution relation in (8) the above relation can be rearranged as

$$\mathcal{D}_{loc,i} = -\frac{\mu_i^v}{2\tau_i}[\bar{\boldsymbol{C}} - \boldsymbol{A}_i^{-1}] : [\bar{\boldsymbol{C}}^{-1} - \boldsymbol{A}_i] \geq 0. \tag{21}$$

To ensure non-negativity of Eqn (21), Linder et al. [29] proved that if $\bar{\boldsymbol{C}}$ is the isochoric part of the right Cauchy-Green tensor and $\boldsymbol{A}_i$ is the symmetric tensorial internal variable of the developed micromechanical polymer model, then the following inequality holds

$$[\bar{\boldsymbol{C}} - \boldsymbol{A}_i^{-1}] : [\bar{\boldsymbol{C}}^{-1} - \boldsymbol{A}_i] \leq 0. \tag{22}$$

For more on this theorem, see Linder et al. [29]. Once the relation (22) is inserted in Eqn (21), the non-negativeness of the dissipation is fulfilled.

References

[1] Ana Ask, Andreas Menzel and Matti Ristinma, *Phenomenological modeling of viscous electrostrictive polymers*, International Journal of Non-Linear Mechanics, doi:10.1016/j.ijnonlinmec.2011.03.020

[2] A. F. M. S. Amin, A. Lion, S. Sekita and Y. Okui, *Nonlinear dependence of viscosity in modeling the rate-dependent response of natural and high damping rubbers in compression and shear: Experimental identification and numerical verification*, International Journal of Plasticity, 22:1610-1667, 2006

[3] A. F. M. S. Amin, M. S. Alam and Y. Okui, *An improved hyperelasticity relation in modeling viscoelasticity response of natural and high damping rubbers in compression: Experiments, parameter identification and numerical verification*, Mechanics of Materials, 34:75-95, 2002

[4] A. Vandenbroucke, H. Laurent, N. Aït Hocine, G. Rio, *A hyperelasto-visco-hysteresis model for an elastomeric behaviour: Experimental and numerical investigations*, Computational Materials Science, 48:495-503, 2010

[5] H. Dal and M. Kaliske, *Bergström-Boyce model for nonlinear finite rubber viscoelasticity: Theoretical aspects and algorithmic treatment for the FE method*, Computational Mechanics, 44:809-823, 2009

[6] P. G. de Gennes, *Reptation of a polymer chain in the presence of fixed obstacles*, Journal of Chemical Physics, 55:572-579, 1971

[7] E. Arruda and M. C. Boyce, *A three-dimensional constitutive model for the large stretch behaviour of rubber elastic materials*, Journal of the Mechanics and Physics of Solids, 41:389-412,1993

[8] J. S. Bergström and M. C. Boyce, *Constitutive modeling of the large strain time-dependent behaviour of elastomers*, Journal of the Mechanics and Physics of Solids, 46:931-954, 1998

[9] J. S. Bergström, *Large strain time-dependent behaviour of elastomeric materials* , PhD Dissertation, MIT, USA, 1999

[10] M. Zrida, H. Laurent, G. Rio, S. Pimbert, V. Grolleau, N. Masmoudi, C. Bradai, *Experimental and numerical study of polypropylene behaviour using an hyper-visco-hysteresis constitutive law*, Computational Materials Science, 45:516-527, 2009

[11] Y. C. Fung, *Biomechanics. Mechanical properties of living tissues*, 2nd edition, Springer-Verlag, New York, 1993

[12] K. Sedlan, *Viscoelastisches Materialverhalten von Elastomerwerkstoffen, Experimentelle Untersuchung and Modellbildung (in German)*, PhD Dissertation, Universität Kassel, Germany, 2001

[13] R. Bird, O. Hassager, R. Armstrong, C. Curtiss, *Dynamics of polymer liquids, kinetic theory*, Wiley, New York, USA, 1977

[14] B. D. Coleman and M.E. Gurtin, *Thermodynamics with internal state variables*, Journal of Chemical Physics, 47:597-613, 1967

[15] M. Doi and S. Edwards, *The theory of polymer dynamics*, Clarendon press, Oxford, 1986

[16] M. S. Hoo Fatt, X. Ouyang, *Three-dimensional constitutive equations for Styrene Butadiene Rubber at high strain rates*, Mechanics of Materials 40:1-16, 2008

[17] M. Green and A. Tobolsky, *A new approach to the theory of relaxing polymeric media*, J. Chem. Phy. 65, 93-121, 1946

[18] M. Johlitz, H. Steeb, S. Diebels, A. Chatzouridou, J. Batal and W. Possart, *Experimental and theoretical investigation of nonlinear viscoelastic polyurethane systems*, Journal of Materials Science, 42:9894-9904, 2007

[19] N. Koprowski, M. Johlitz, S. Diebels, *Characterizing the time dependence of filled EPDM*, Rubber Chemistry and Technology 84(2):147-165, 2011

[20] N. Koprowski, M. Johlitz, S. Diebels, *Modelling of a cellular rubber with non-linear viscosity functions*, Experimental Mechanics 51:749-765, 2011

[21] N. Huber, C. Tsakmakis, *Finite deformation viscoelasticity laws*, Mechanics of Materials 32:1-18, 2000

[22] C. Miehe, S. Göktepe and F. Lulei, *A Micro-macro approach to rubber-like materials: Part-I, the non-affine micro-sphere model of rubber elasticity*, Journal of the Mechanics and Physics of Solids, 52:2617-2660, 2004

[23] C. Miehe and S. Göktepe, *A micro-macro approach to rubber-like materials: Part-II, the micro-sphere model of finite rubber viscoelasticity*, Journal of the Mechanics and Physics of Solids, 53:2231-2258, 2005

[24] G. A. Holzapfel, *Nonlinear Solid Mechanics: A Continuum Approach for Engineering*, Wiley & Sons Ltd, UK, 2000

[25] S. Reese and S. Govindjee, *A theory of finite viscoelasticity and numerical aspects*, International Journal of Solids and Structures, 35:3455-3482, 1998

[26] G. Marckmann, E. Verron, *Comparison of hyperelastic models for rubberlike materials*, Rubber Chemistry and Technology, 79:835-858, 2006

[27] D. K. Vu, P. Steinmann and G. Possart, *Numerical modeling of non-linear electroelasticity*, International Journal for Numerical Methods in Engineering, 70:685-704, 2007

[28] D. K. Vu, P. Steinmann, *A 2-D coupled BEM-FEM simulation of electroelastostatics at large strain*, Computer Methods in Applied Mechanics and Engineering, 199:1124-1133, 2010

[29] C. Linder, M. Tkachuk and C. Miehe, *A micromechanically motivated diffusion-based transient network model and its incorporation into finite rubber viscoelasticity*, Journal of the Mechanics and Physics of Solids, 59:2134-2156, 2011

[30] J. Lubliner, *A model of rubber viscoelasticity*, Mechanics Research Communications, 12(2):93-99, 1985

[31] G. Holzapfel, J. Simo, *A new viscoelastic constitutive model for continuous media at finite thermodynamical changes*, International Journal of Solids and Structures, 33:3019-3034, 1996

[32] M. Hossain, *Modelling and computaion of polymer curing*, PhD Dissertation, University of Erlangen-Nuremberg, Germany, 2010

[33] P. Steinmann, M. Hossain and G. Possart, *Hyperelastic models for rubber-like materials: Consistent tangent operators and suitability of Treloar's data*, Archive of Applied Mechanics, Accepted, 2012

[34] M. Kaliske, H. Rothert, *Formulation and implementation of three-dimensional viscoelasticity at small and finite strains*, Computational Mechanics 19, 228-239, 1997

[35] J. C. Simo, *On a full three dimensional finite strain viscoelastic damage model: formulation and computational aspects*, Compututer Methods in Applied Mechanics and Engineering 60, 153-173, 1987

[36] A. Lion, *A physically based method to represent the thermo-mechanical behaviour of elastomers*, Acta Mechanica 123, 1-25, 1997

[37] M. Wissler, E. Mazza, *Mechanical behaviour of an acrylic elastomer used in dielectric elastomer actuators*, Sensors and Actuators A 134, 494-504, 2007

[38] Z. Gao, A. Tuncer, A. H. Cuitino, *Modeling and simulation of the coupled mechanical-electrical response of soft solids*, International Journal of Plasticity 27(10), 1459-1470, 2011

[39] A. Büschel, S. Klinkel, W. Wagner, *A viscoelastic model for dielectric elastomers based on a continuum mechanical formulation and its finite element implementation*, Proceedings SPIE 7976, 79761R (2011)

COMMAT-S-12-00133

Overview of revisions incorporated into

Experimental study and numerical modelling of VHB 4910 polymer

by

Mokarram Hossain, Duc Khoi Vu and Paul Steinmann

(submitted to Computational Materials Science, 2012)

As per reviewer comments and suggestions, revisions in the manuscript are given in blue color and comments from the authors are given subsequently (red coloured)

Reviewer 1:

- Since the authors only investigated and modelled mechanical material properties, the keywords "electro-active polymer" and "electro-mechanical coupling" should be omitted in the revised version.
  -Keywords have been changed
  VHB 4910, viscoelasticity, micro-mechanical model

- In line 53 on page 2, it should read: "...that are sometimes difficult to identify".
  -The sentence has been changed
  ...that are sometimes difficult to identify.

- In line 49 on page 9, it should read: "...carried out to produce more data in order to...".
  -The sentence has been changed
  ...carried out to produce more data in order to...

- In eq. (1) and also on the left-hand side of eq. (2) the authors should introduce more internal state variables: $\Psi = \tilde{\Psi}(\boldsymbol{C}, \boldsymbol{A}_1, \cdots, \boldsymbol{A}_s)$
  -The equation has been changed

$$\Psi = \tilde{\Psi}(\boldsymbol{C}, \boldsymbol{A}_1, \cdots, \boldsymbol{A}_s) \tag{23}$$

where s denotes the number of elements which form the relaxation spectrum.

- It is not necessary, that the internal state variables of the specific Helmholtz free energy are of the strain type and these of the specific Gibbs free energy are of the stress type. Thus it is proposed to delete the formulation "strain-like" in line 47 of page 13.
  -The phrase "strain-like" has been removed

- In line 9 on page 14, it should read: "... and s denotes the number of elements which form the relaxation spectrum". On the same page, in line 18, it should read: "In Eqn. (3), we have...".
  -The sentence has been modified
  In Eqn. (3), we have...

- Although the formulation "fictitious stress tensor" is occasionally used in the literature, the reviewer proposes to avoid it. It is a stress tensor which arises when the volumetric isochoric split if the deformation gradient is introduced.
  -The word "fictitious" has been removed

- On page 16 in line 19, it should read "...due to the stress-free boundary conditions, both... ".
  -The sentence has been modified
  ...due to the stress-free boundary conditions, both...

- In line 10 on page 20, it should read: "Maxwell element produces two extra...". On the same page in line 14, it should read :"the number of Maxwell elements..."
  -Both sentences have been modified
  Maxwell element produces two extra...
  "the number of Maxwell elements...

- In the context of eqs. (7) - (9) it would be helpful for the reader who is not familiar with finite viscoelasticity to show that the dissipation of the viscoelastic part of the model is nonnegative (perhaps in the appendix).

-In order to show the thermodynamical consistency of the applied constitutive model, following paragraph has been added as an Appendix in the revised version

Appendix A: Thermodynamical consistency of the viscoelastic model

The constitutive relations presented in Eqns (7-9) are required to fulfill the entropy inequality, which, if only isothermal processes are considered, is equal to the so-called dissipation inequality, i.e.

$$\boldsymbol{S} : \frac{1}{2}\dot{\boldsymbol{C}} - \dot{\Psi} \geq 0. \tag{24}$$

If one performs the time derivative of the total energy, i.e. $\tilde{\Psi}(\boldsymbol{C}, \boldsymbol{A}_1, \cdots, \boldsymbol{A}_s)$ and inserts it in Eqn (24), we obtain

$$\left[\boldsymbol{S} - 2\frac{\partial \Psi}{\partial \boldsymbol{C}}\right] : \frac{1}{2}\dot{\boldsymbol{C}} - \sum_{i=1}^{s} \frac{\partial \Psi}{\partial \boldsymbol{A}_i} : \dot{\boldsymbol{A}}_i \geq 0. \tag{25}$$

To obtain a thermodynamically consistent formulation that obeys the second axiom of thermodynamics the local dissipation has to be non-negative, which, due to Coleman and Gurtin argumentation [14] yields

$$\mathcal{D}_{loc} = -\sum_{i=1}^{s} \frac{\partial \Psi}{\partial \boldsymbol{A}_i} : \dot{\boldsymbol{A}}_i = -\sum_{i=1}^{s} \frac{\partial \bar{\Psi}^{v}_{iso,i}}{\partial \boldsymbol{A}_i} : \dot{\boldsymbol{A}}_i = \sum_{i=1}^{s} \mathcal{D}_{loc,i} \geq 0. \tag{26}$$

Performing the derivation of the viscous part of the energy function from Eqn (7) along with the evolution relation in (8) the above relation can be rearranged as

$$\mathcal{D}_{loc,i} = -\frac{\mu_i^v}{2\tau_i}[\bar{\boldsymbol{C}} - \boldsymbol{A}_i^{-1}] : [\bar{\boldsymbol{C}}^{-1} - \boldsymbol{A}_i] \geq 0. \tag{27}$$

To ensure non-negativity of Eqn (27), Linder et al. [29] proved that if $\bar{\boldsymbol{C}}$ is the isochoric part of the right Cauchy-Green tensor and $\boldsymbol{A}_i$ is the symmetric tensorial internal variable of the developed micromechanical polymer model, then the following inequality holds

$$[\bar{\boldsymbol{C}} - \boldsymbol{A}_i^{-1}] : [\bar{\boldsymbol{C}}^{-1} - \boldsymbol{A}_i] \leq 0. \tag{28}$$

For more on this theorem, see Linder et al. [29]. Once the relation (28) is inserted in Eqn (27), the non-negativeness of the dissipation is fulfilled.